Predictions of Hole Mobilities in Oligoacene Organic Semiconductors from Quantum Mechanical Calculations†

Wei-Qiao Deng and William A. Goddard III*

Materials and Process Simulation Center, California Institute of Technology, Pasadena, California 91125

Received: January 29, 2004; In Final Form: April 21, 2004

We estimate the hole mobility for oligoacene crystals using quantum mechanics (QM) to calculate the reorganization energy and electron-transfer coupling matrix elements and molecular dynamics (MD) to do the thermal averaging. Using an incoherent transport model we calculate a hole mobility of 6.5 $cm^2/(V\ s)$ for pentacene crystals at 300 K. This can be compared to recent experimental results of 5 $cm^2/(V\ s)$. However, we find that an alternative packing into the crystal could lead to a hole mobility of 15.2 $cm^2/(V\ s)$. This suggests that current materials might still be improved by a factor of ∼3. Such calculations might be useful for finding solid-state structures that would increase the hole mobility for use in high-performance molecular devices.

1. Introduction

There is a great deal of interest in developing materials suitable for cheap, flexible electronic devices (e.g., Smart Card, flexible displays). A critical problem here is achieving the ∼10 $cm^2/(V\ s)$ hole mobility required for integrated circuits based on organics.[4] Amorphous Si is sufficient but too expensive. Organic semiconductors could ultimately be cheap enough, but the mobilities are low (10^{-2} $cm^2/(V\ s)$ for amorphous pentacene and up to 5 $cm^2/(V\ s)$ in thin films).[1−3] Moreover, many display and memory applications require much faster devices and hence higher mobilities. This raises the question of whether additional modifications in the engineering design of organic semiconductors could improve performance by the factors required.[3]

To investigate this issue, we developed a quantum mechanical (QM) protocol to estimate the mobilities for organic crystals as a function of temperature and pressure and applied it to four oligoacenes (pentacene, tetracene, anthracene, and naphthalene) with structures shown in Figure 1. Our estimates suggest that for the bulk crystal the limiting mobility at 300 K is ∼6.5 $cm^2/(V\ s)$ for atmospheric pressure, indicating that the current materials are close to the optimum. We suggest that these approaches to computational estimates may be useful for virtual screening to find new lead materials likely to provide the improved properties required for increased transport efficiency (for increased device speed), reduced power, and avoidance of excessive heating in the promising new applications.

Section 2 describes the theoretical methodology, including calculations of reorganization energy, coupling matrix elements, and the incoherent transport model. Section 3 discusses the results calculated for the four oligoacenes. The conclusions are presented in section 4.

2. Theoretical Methodology

The charge carrier mobility provides the figure of merit for applications of organics in electronic devices. For p-type oligoacene derivatives the conductivity is dominated by transport of positive charges (holes) with mobilities (μ) in the range 10^{-2}−10 $cm^2/(V\ s)$ reported for the thin film and crystalline phases of pentacene.[1−4] Unfortunately, there remain conflicts between experimental measurements,[6] making it essential to develop a solid theoretical basis for understanding the mechanisms dominating hole mobility.

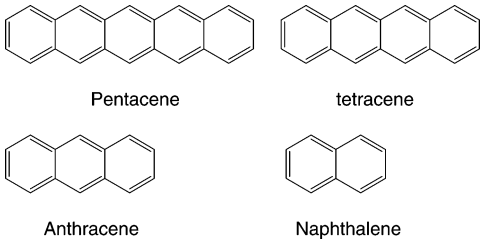

Figure 1. Chemical structures of several oligoacenes.

Electronic band structure calculations have previously been used to predict charge transport in perfect crystals of pentacene. Cheng et al. carried out band calculations for oligoacenes, which, assuming a coherent model, they used to predict thermal-averaged velocity−velocity tensors. Comparing these tensors to recent experimental data they concluded that the simple band model is unable to explain the temperature dependence of the charge carrier mobility in oligoacene crystal systems for temperatures higher than 150 K.[5] This suggests that dynamic structure disorder may invalidate the band transport model for temperatures above 150 K, suggesting that hopping may be the dominant mechanism at room temperature.

Structural disorder decreases the charge carrier mobility, giving rise to photocurrent transients and frequency dependence in the charge carrier mobility. The disorder leads to a nonperiodic structure that may cause the transport mechanism to switch from band-like transport at low temperature (little disorder) to a hopping mechanism at higher temperature. Here structural fluctuations resulting from twisting and sliding of the molecules could play a prominent role.

To obtain quantitative insight into the role of structural disorder on the mobility of charge carriers in pentacene, we

† Part of the special issue "Alvin L. Kwiram Festschrift".

* To whom correspondence should be addressed. E-mail: wag@wag.caltech.edu.

10.1021/jp0495848 CCC: $27.50
Published on Web 06/02/2004

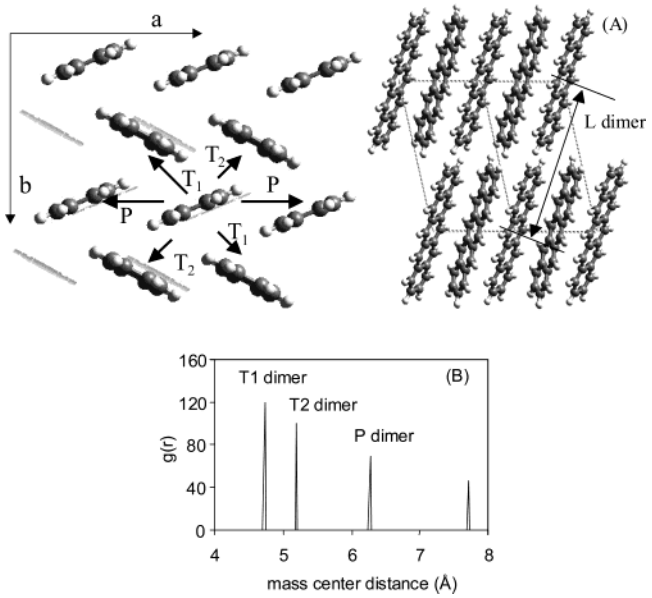

Figure 2. Crystal structure of the pentacene crystal, a typical oligacene: (A) dimer type neighbors in the crystal; (B) radial distribution function for the different dimer types.

use an incoherent hopping model to describe the hole mobilities of oligoacenes at room or higher temperatures. Our aims are

- to provide a simple way to predict accurate values of the coupling matrix elements and reorganization energies involved in hole transport and
- to obtain a dynamical model useful for predicting absolute hole mobilities based on first principles results.

Incoherent and partially coherent processes including effects of dynamic or static structural fluctuations have been used to estimate hole mobilities in liquid crystals.[8−10] However, such approaches have not yet been applied to estimate hole mobilities oligoacene systems.

2.1. Transport Properties. To describe charge transport in oligoacenes, we consider an incoherent hopping model in which charge can transfer only between adjacent molecules. A similar approach was used successfully to describe the conduction properties of organic superconductors.[27]

Figure 2 shows the several different types of dimers in the pentacene crystal:

- transverse dimers at distances of $T_1 = 4.75$ Å (two) and $T_2 = 5.25$ Å (two)
- parallel dimers at distance of $P = 6.253$ Å (two)
- longitudinal dimers at $L = 14.51$ Å (two)

Viewing each hopping event as a nonadiabatic electron-transfer reaction, we use standard Marcus theory to express the rate of charge motion between neighboring molecules, W, in terms of the reorganization energy λ and the coupling matrix element V. Assuming that the temperature is sufficiently high that vibrational modes can be treated classically, we obtain[10]

$$W = \frac{V^2}{\hbar}\left(\frac{\pi}{\lambda k_B T}\right)^{1/2} \exp\left(-\frac{\lambda}{4k_B T}\right) \tag{1}$$

where k_B is the Boltzmann constant and T is the temperature. Given the hopping rate between two neighbors, the diffusion coefficient can be evaluated from the hopping rates as

$$D = \frac{1}{2n}\sum_i r^2 W_i P_i \tag{2}$$

where $n = 3$ is the dimensionality, W_i is the hopping rate due to charge carrier to the ith neighbor, r_i is the distance to neighbor i, P is the relative probability for charge carrier to a particular ith neighbor,

$$P_i = W_i / \sum_i W_i \tag{3}$$

Summing over all possible hops leads to the diffusion coefficient in eq 2. The drift mobility of hopping, μ, is then evaluated from the Einstein relation,

$$\mu = \frac{e}{k_B T} D \tag{4}$$

where e is the electronic charge.

Considering now the structural disorder present at higher temperature, the coupling matrix element V becomes a function of distance between two adjacent molecules, leading to

$$W(r) = \frac{V(r)^2}{\hbar}\left(\frac{\pi}{\lambda k_B T}\right)^{1/2} \exp\left(-\frac{\lambda}{4k_B T}\right) \tag{5}$$

Here we neglect the angular changes between the dimers. The relative probability in eq 3 becomes

$$P(r) = N(r)\, W(r) / \int_0^\infty N(r)\, W(r)\, \mathrm{d}r \tag{6}$$

where the $N(r)$ is the number of near neighbors at r

$$N(r) = \rho g(r) 4\pi r^2\, \mathrm{d}r \tag{7}$$

and $g(r)$ is the probability density of having this type of neighbor at a distance r.

The resulting diffusion coefficient becomes

$$D = \frac{1}{2n}\int_0^r r^2 W(r)\, P(r)\, \mathrm{d}r \tag{8}$$

The hole mobility is still be evaluated by eq 4.

2.2. Reorganization Energy λ. Assuming that the "hole-containing" (charged) molecule M is at its equilibrium geometry, M_e^+, and that the neutral molecule P is at its equilibrium geometry, P_e, then after the charge transfer the now neutral molecule would relax to the equilibrium geometry M_e whereas the now charged molecule would relax to P_e^+. This *reorganization energy*,[11] λ, can be partitioned into two parts:

- *fast changes* due to relaxation in the molecular geometry (*inner sphere* contribution) and
- *slow changes* due to repolarization of the surrounding solvent medium (*outer sphere* contribution)

We will neglect the outer sphere contributions to focus on the structural differences between the equilibrium configurations of π-conjugated units. We expect to provide absolute values of hole mobility in such a system that can catch the major contributions and be comparable to experimental measurement.

Figure 3 illustrates the calculation of the reorganization energy. For each oligoacene molecule, the geometry was optimized using quantum mechanics (QM) for both neutral and ionic states as shown in Figure 3. Accordingly, the elementary hopping step in molecular wires is characterized by four energies: E (neutral in neutral geometry), E^* (neutral in ion geometry), E_+ (ion in ion geometry), and E_+^* (ion in neutral geometry). By definition,[11,12]

$$\lambda = \lambda_1 + \lambda_2 = (E_+^* - E_+) + (E^* - E) \tag{9}$$

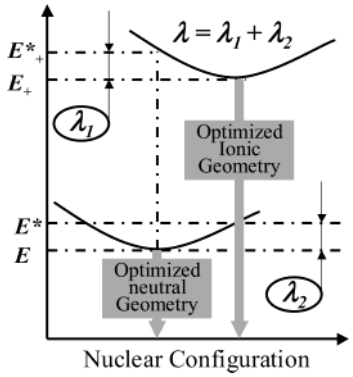

Figure 3. Schematic diagram for the Marcus−Hush calculation of reorganization energy.

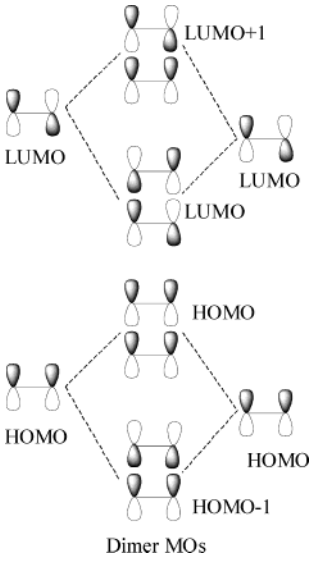

Figure 4. Diagram for the estimate of coupling matrix elements in the neutral dimer.

In addition to reorganization energy, the vertical ionization potential (VIP) is also determined by Figure 3.[11]

$$\mathrm{VIP} = E^*_+ - E \tag{10}$$

The QM calculations to determine these quantities used the B3LYP flavor of density functional theory (DFT) with the 6-311G** triple-ζ-single polarization basis set.[13] All calculations on open shell (ionized) states used the unrestricted formalism (UB3LYP), but spin contamination was minimal (less than 0.01).

2.3. Coupling Matrix Element *V*. We calculated the electron-transfer coupling matrix element, *V*, between adjacent molecules within the framework of the Marcus−Hush two-state model,[11,14] as sketched in Figure 4. Thus the coupling matrix element for a given electronic level is related to the energetic splitting of that level in the dimer as compared to the isolated neutral molecule. For these organics the highest occupied molecular orbital (HOMO) of the isolated molecule is a π orbital delocalized over the molecule (with energy ϵ), which for the neutral dimer splits into two levels denoted as HOMO and HOMO−1. The coupling matrix element, *V*, is given by

$$V = \frac{1}{2}\sqrt{(E_{\mathrm{HOMO}} - E_{\mathrm{HOMO-1}})^2 - (\epsilon_2 - \epsilon_1)^2} \tag{11}$$

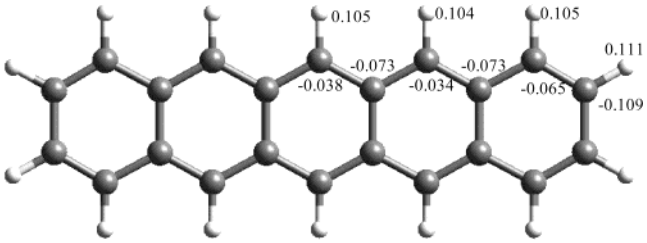

Figure 5. QM charges for the neutral pentacene molecule.

TABLE 1: Optimum Crystal Cell Parameters for Pentacene from Experiment,[19] MD at 300 K and from Minimization

	experiment (300 K)	MD (300 K)	minimized
A (Å)	6.275	5.950	6.243
B (Å)	7.714	8.423	7.485
C (Å)	14.442	17.445	16.052
α	76.75°	94.76	69.3°
β (deg)	88.01°	112.57	81.68°
γ (deg)	84.52°	91.24	86.16°
cell density (g/cm^3)	1.3649	1.2348	1.3317

In this case the isolated molecules are identical (and in equivalent sites in the crystal), so that eq 11 becomes

$$V = \frac{1}{2}(E_{\mathrm{HOMO}} - E_{\mathrm{HOMO-1}}) \tag{12}$$

The quantities used in (9) and (12) were obtained from QM calculations as indicated in section 2.2.

2.4. Molecular Dynamics. To obtain the thermal fluctuations in the hopping matrix elements for a given temperature and pressure, we carried out MD simulations (using Cerius2[15]). Here we considered a 3 × 3 × 2 supercell with 36 pentacene molecules. We used the Dreiding force field (FF)[16] (reported to be effective for pentacene[17]) with the Lennard-Jones 12-6 description of vdW interactions and (Mulliken) charges from QM populations (shown in Figure 5). The simulations were carried out in the canonical ensemble (NPT), using the Nose−Hoover thermostat (relaxation time constant 0.1 ps) to maintain the temperature *T* and the Rahman−Parrinello barostat (mass factor 1.0) to maintain the pressure *P*. The electrostatic interactions were calculated using the ABCA formalism for Ewald summations.[18]

The cell parameters from minimization and from MD at 300 K are compared with the 300 K experimental values[19] in Table 1. The densities at 300 K differ by 2.4%.

We carried out two series of simulations.

- To obtain the temperature dependence, we considered 250, 300, 350, and 400 K all at 0.0001 GPa (∼1 atm) pressure.
- To obtain the pressure dependence, we considered pressures of 0.0001, 0.1, 0.5, and 1.0 GPa all at 300 K.

Each simulation was 100 ps with the measurements over the last 50 ps.

3. Results and Discussion

3.1. Reorganization Energy and Coupling Matrix Element. The QM optimized structures for the neutral and oxidized forms of naphthalene, anthracene, tetracene, and pentacene are presented in Figure 6. All neutral and oxidized molecules stay planar [for pentacene the lowest frequency (out-of-plane) is 46.75 cm^{-1}]. We see a consistent trend in the alternation of the bond lengths and bond angles due to ionizing the HOMO. Naphthalene shows the largest geometry relaxations, with

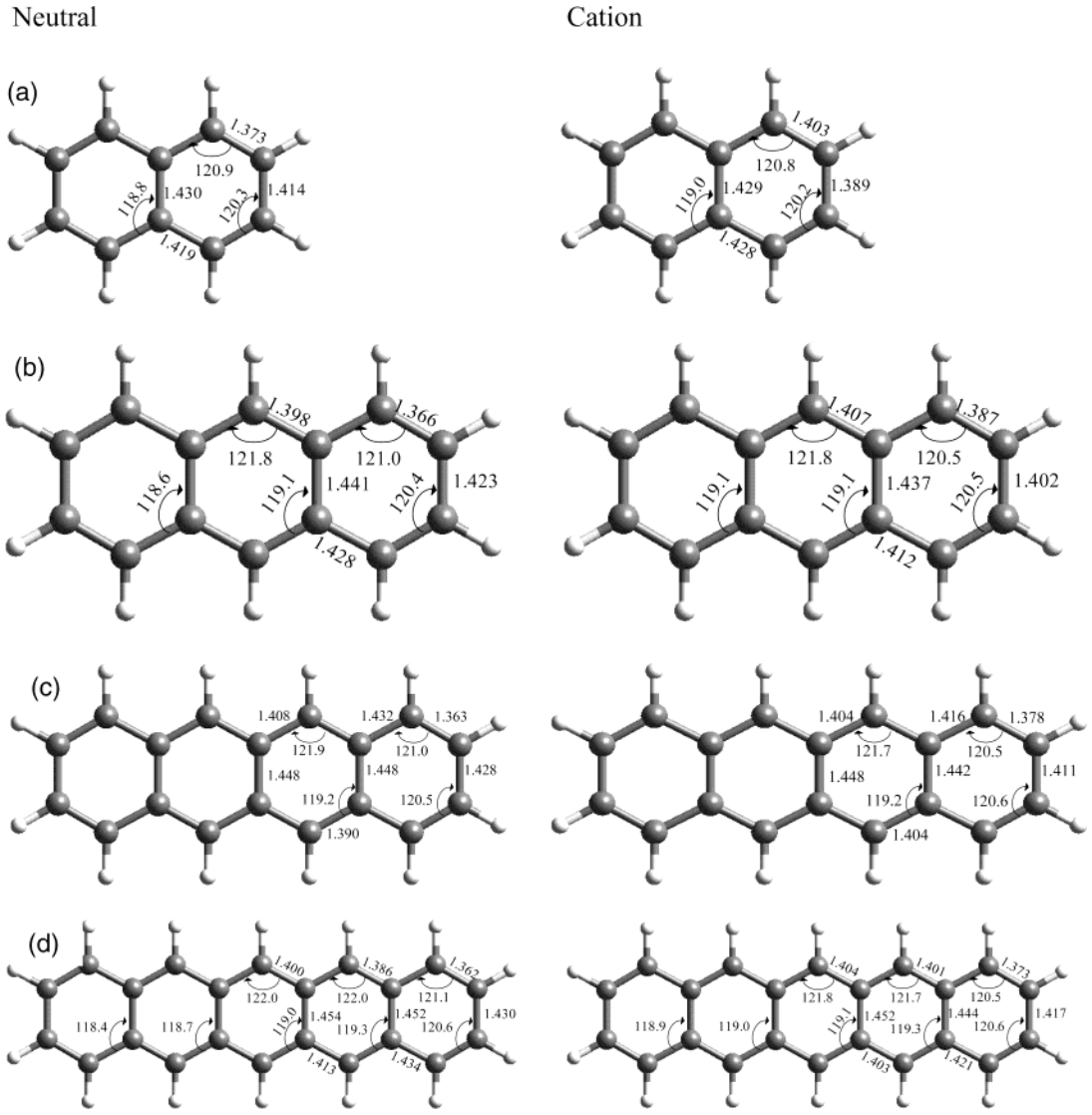

Figure 6. Structural data from QM calculations of the neutral and cation states of oligoacenes: (a) naphthalene; (b) anthracene; (c) tetracene; (d) pentacene.

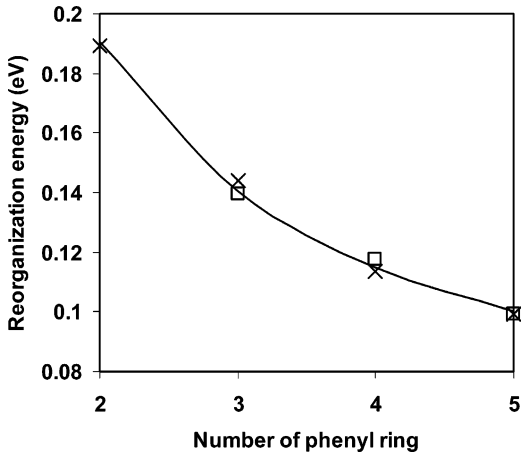

Figure 7. Reorganization energy versus the number of phenyl rings. The calculated values are indicated by crosses, and the experimental numbers are indicated by squares. The line is based on $\lambda = 0.0395 - 0.3024/N$ (eV).

changes in C−C bond lengths on the order of 0.030 Å, leading to the largest reorganization energy of 0.1893 eV. Pentacene has the smallest geometry relaxations, with changes in C−C bond lengths on the order of 0.01 Å, leading to the smallest reorganization energy of $\lambda = 0.0993$ eV. This is in excellent agreement with the value of $\lambda = 0.0992$ eV[20] deduced from experiment. As summarized in Table 2 and Figure 7, the increased charge delocalization with increased number of conjugated phenyl rings, N, leads to a reorganization energy that decreases uniformly as

$$\lambda = 0.0395 - 0.3024/N \text{ (eV)} \qquad (13)$$

The calculated vertical ionization potentials (Table 2) are 2−6% lower than experimental results.[21]

The crystal structure leads to the four types of dimers; T_1, T_2, P, and L shown in Figure 2. The T_1 dimer is closest at 4.7 Å with a cross angle of ~51.9°, as shown in Figure 8a. The T_2 dimer is at ~5.13 Å with a cross angle of 52° but with a slide shift of 2.46 Å, as shown in Figure 8b. The P dimer has adjacent molecules at 6.25 Å distance and parallel, but this displacement is at an angle of 53° from the normal to the molecular plane, as in Figure 8c. The L dimer has neighbors at 14.10 Å and almost parallel as in Figure 8d. The geometries of the dimer structures were optimized (B3LYP/6-311G**) with the center mass distance and cross-angle plane fixed.

TABLE 2: QM Energies (Hartree) for Each Structure Calculated from QM (UB3LYP/6-311G)[a]**

		naphthalene	anthracene	tetracene	pentacene
E (hartree)		−385.98524	−539.65551	−693.32308	−846.98975
E^* (hartree)		−385.98185	−539.65299	−693.32099	−846.98774
E_+ (hartree)		−385.69769	−539.39689	−693.08378	−846.76430
E_+^* (hartree)		−385.69413	−539.39413	−693.08171	−846.76267
VIP[a] (eV)	this work	7.9286	7.1190	6.5740	6.1845
	experiment	8.144[b]	7.202[b]	6.97[b]	6.63[b]
λ[a] (eV)	this work	0.1893	0.1441	0.1135	0.0993
	experiment		0.1394[c]	0.1176[c]	0.0992[c]

[a] The vertical ionization potential (VIP) and reorganization energy (λ). [b] NIST database.[21] [c] Podzorov, V.; et al.[26]

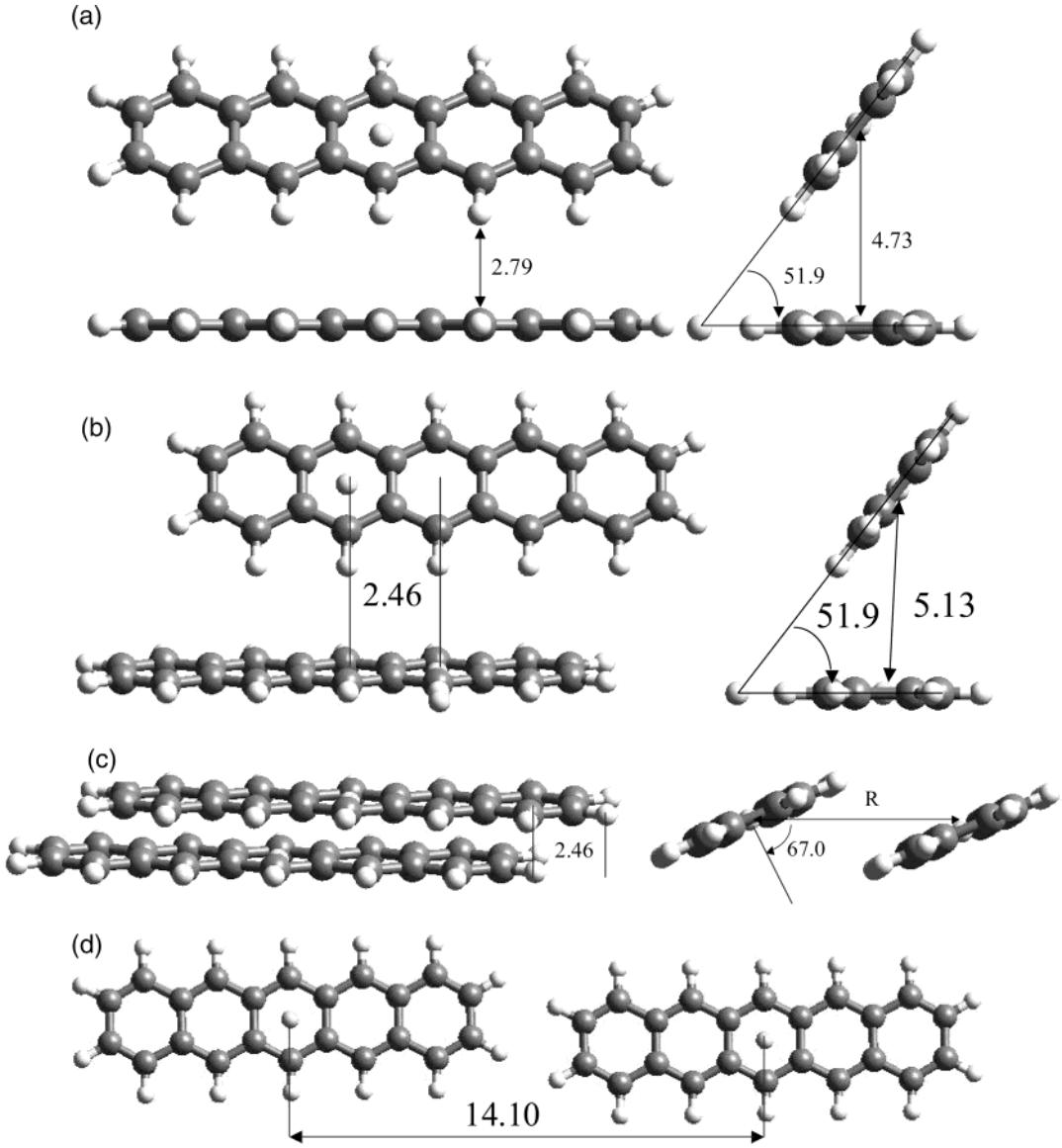

Figure 8. QM structures for various dimers. (a) Front view and side view of the T_1 dimer. The yellow atoms are dummy atoms for convenience in defining angles and distances. The structure was optimized by fixing the planar angle at 51.9° and the center of mass (CM) distance at 4.73 Å. (b) Front view and side view of the T_2 dimer. The CM is slid away by 2.46 Å, and the CM distance is 5.13 Å. (c) Front view and side view of the P dimer. The mass center distance is 6.25 Å., which is at an angle of 67° from the normal to the molecule. (d) Front view of the L dimer. The CM distance is 14.10 Å.

For the pentacene dimer, the coupling in the T_1 dimer (V = 0.137 eV) and T_2 (0.120 eV) are far larger than for P (0.006 eV) and L (0.0008 eV). Thus P and L dimers contribute little to hole mobility. This indicates that the hole mobility is quite anisotropic and dominated by hole transfer within the layers, which is consistent with experiment.[22] Of course, the coupling depends on the distance between the dimers, as shown in Figure 9 for the T_1 and P dimers. Even at the same distance, the P dimer has a much smaller coupling than the T_1 dimer. For example, the coupling in the T_1 dimer with 4.734 Å (and a cross angle of ∼51.9°) is 0.137 eV, but it decreases to 0.105 when the two phenyl rings are parallel to each other with the same CM distance of 4.734 Å. This is because the orbitals of the T_1 dimer can couple through the hydrogen atoms that penetrate close to the pentacene face of the dimer partner. On the other hand, the P dimer becomes much more stable than the T_1 dimer

TABLE 3: Calculated Properties of Oligoacenes

		naphthalene	anthracene	tetracene	pentacene
T_1 dimer CM distance (Å)		5.078	5.188	4.774	4.734
V_{T1} (eV)		0.114	0.0986	0.136	0.137
T_2 dimer CM distance (Å)		5.078	5.188	5.126	5.199
V_{T2} (eV)		0.114	0.0986	0.118	0.120
P dimer CM distance (Å)		5.973	6.000	6.030	6.253
V_p (eV)					0.006
L dimer CM distance (Å)		8.675	11.12	13.53	14.10
V_L (eV)					0.0008
diffusion coefficient, D (cm^2/s)		0.0342	0.0477	0.1096	0.1387
drift mobility, μ [$cm^2/(V\ s)$]	this work	1.32	1.84	4.24	5.37
	experiment	0.4−1[a]	0.57−2.07[b]	0.14,[c] 0.4[d]	3,[e] 5−7[f]

[a] Karl, N.; et al.[6] [b] Silinsh E. A.; et al.[7] [c] Butko, V. Y.; et al.[23] [d] de Boer, R. W. I.; et al.[24] [e] Klauk, H.; et al.[4b] [f] Kelley, T. W.; et al.[4a]

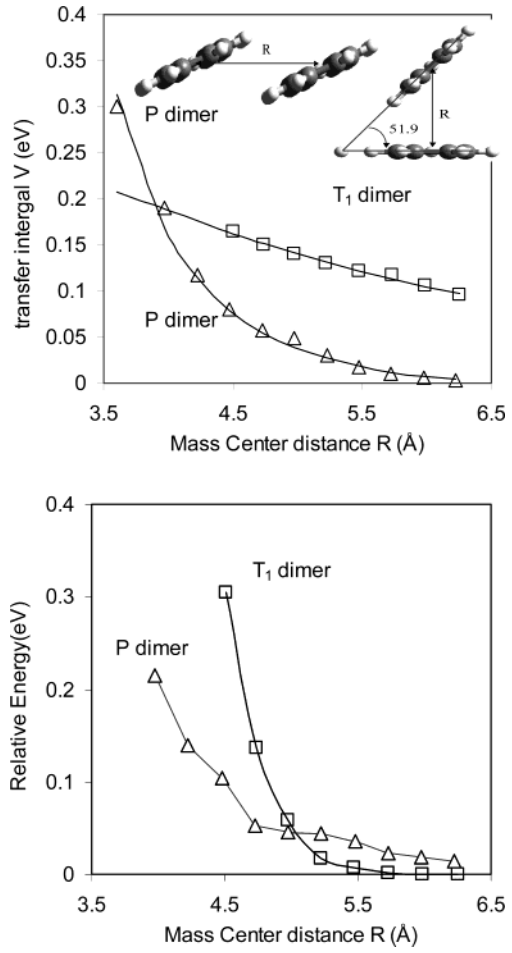

Figure 9. Dependence of coupling matrix elements (calculated using B3LYP/6-311G**) on the CM distance. For the T_1 dimer the 51.9° angle is kept fixed while the R is varied (squares are quantum mechanic data; the curve is based on fitting equation as $|V(r)| = 0.4708 - 0.0912r + 0.0050r^2$). For the P dimer the two molecules are kept parallel while the R is varied (triangles are QM data; the curve is based on fitting equation $|V(r)| = -0.0078 + 697.0/r^6 + 0.3252/r^{12}$).

when the CM is less than 4.9 Å and the coupling of the P dimer becomes larger than T_1 dimer whereas the CM is less than 3.9 Å. Indeed, at the optimum distance of 3.6 Å the coupling is 0.30 eV.

Considering all four oligocenes, the largest coupling matrix elements V are all in the range from 0.10 to 0.13 eV. Because the observed mobilities differ by over a factor of 10, the coupling matrix element term may not be the only important factor in determining hole transport.

TABLE 4: Experimental Cell Parameters Used in Matrix Element Calculations[19]

	naphthalene[19a]	anthracene[19b]	tetracene[19c]	pentacene[19d]
space group	$P_{21/a}$	$P_{21/a}$	$P\bar{1}$	$P\bar{1}$
A (Å)	8.213	8.467	6.057	6.275
B (Å)	5.973	5.999	7.838	7.714
C (Å)	8.675	11.124	13.010	14.442
α (deg)	90.00	90.00	77.13	76.75
β (deg)	123.39	125.06	72.12	88.01
γ (deg)	90.00	90.00	85.79	84.52
cross angle (deg)	52.3	51.1	51.3	51.9

3.2. Transport Properties. The diffusion coefficient and the drift mobility of holes in oligoacene were estimated from eqs 1−4 using the internal reorganization energies and the coupling matrix elements based on QM.

3.2.1. Mobility Estimate Based on Minimized Crystal Structures. First we ignore structural disorder at ambient conditions. For pentacene this leads to $\mu = 5.37$ $cm^2/(V\ s)$, which compares well with the experimental values of 3−7 $cm^2/(V\ s)$[4] measured for thin films, which we assume to be ordered much as in the crystal. [Current experiments on "single crystals" lead to much smaller values, ∼0.01 $cm^2/(V\ s)$, which we assume to arise from numerous defects in the "single crystals".] However, for tetracene we find $\mu = 4.24$ $cm^2/(V\ s)$, which is much larger than current experiments 0.15−0.4 $cm^2/(V\ s)$.[23,24] Because the reorganization energies (both experimental and theoretical) and coupling matrix elements of tetracene and pentacene are similar, we conclude that *the current experimentally mobility of tetracene is only 1/10th of its optimum value so that further effort could likely improve the hole mobility by a factor of 10.*

3.2.2. Estimate Based on Molecular Dynamics. As the temperature increases, structural disorder modifies the matrix elements, changing the hole mobility for the system. To predict these changes, we use eqs 5−8 to calculate the hole mobilities as a function of temperature.

We carried out NPT MD simulations for pentacene at temperatures of 250, 300, 350, and 400 K (with 1 atm pressure). These calculations require the radial distribution function as a function of temperature as shown in Figure 10. As the temperature increases, the populations of T_1 and T_2 dimers decrease, leading to reduced hole mobilities, as shown in Figure 11. The calculated hole mobility behaves as $\mu \sim T^{-0.57}$. Note added in proof: A recent calculation (Kannewald, K.; Bobbert, P. A. *Phys. Rev. B* **2004**, *69*, 075212) reports a temperature dependence of $\sim T^{-0.5}$ near 300 K, in good agreement with our value.

We also carried out MD simulations at pressures of 1 atm and 0.1, 0.5, and 1 GPa all at 300 K. As the pressure increases, we find that the T_1 type dimer distance decreases whereas the

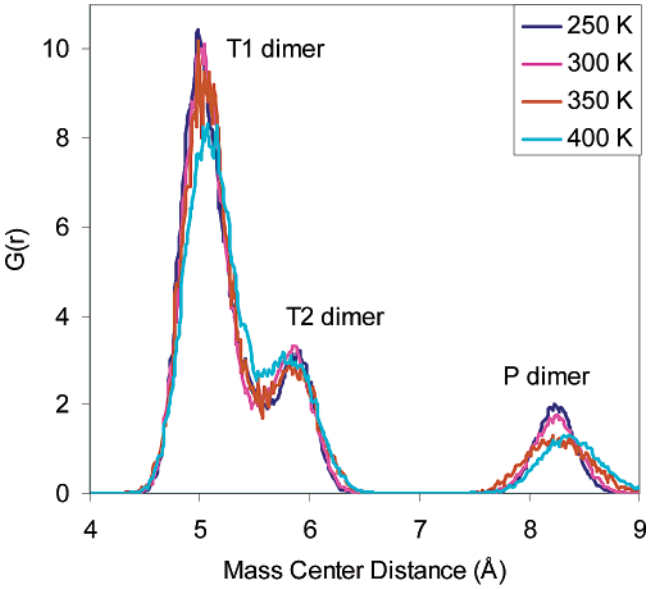

Figure 10. Radial distribution $g(r)$ of pentacene calculated from MD simulations as a function of temperature (1 atm).

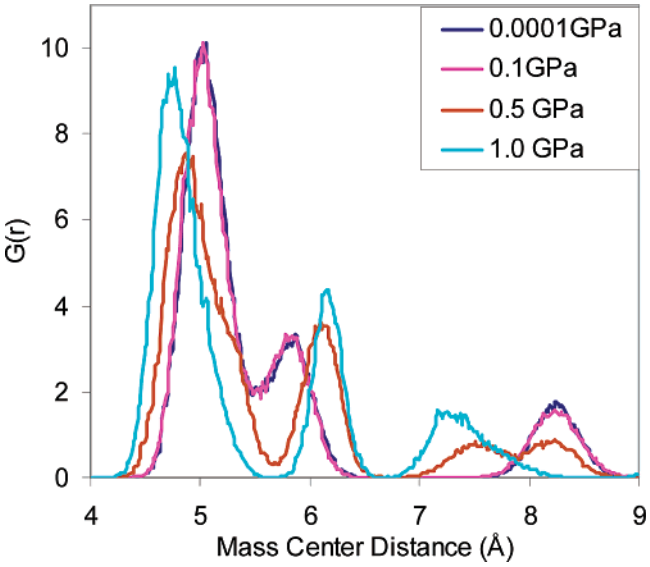

Figure 12. Radial distribution $g(r)$ of pentacene calculated from MD simulation at different pressures (300 K).

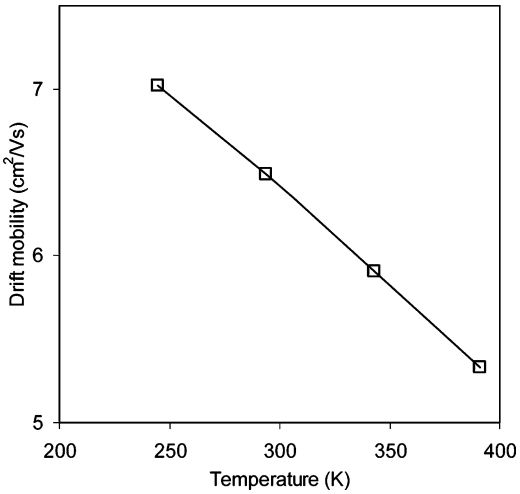

Figure 11. Drift mobility calculated for pentacene as a function of temperature.

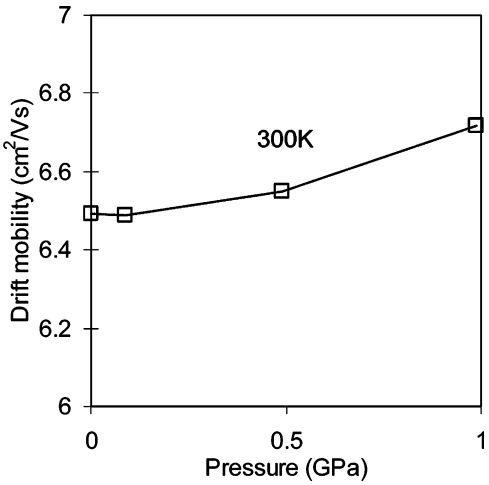

Figure 13. Drift mobility calculated for pentacene as a function of pressure.

T_2 type distance increases. The calculated distribution functions are shown in Figure 12. This leads to the calculated hole mobilities shown in Figure 13, indicating that the hole mobilities increase with increased external pressure. However, change is less than a factor of 1.4 times, suggesting that merely changing the pressure will not dramatically increase hole mobilities of pentacene.[25]

3.3. Toward Higher Hole Mobilities. Many efforts are being made to improve the hole mobility of pentacene by using different substrates, different deposition methods, etc. These efforts are generally directed toward changing the crystal packing to obtain a phase with higher mobility. Here we will use our simple transport model (with the hole mobilities governed by just two parameters: coupling matrix element and reorganization energy) to discuss several possibilities for improving mobilities via modified crystal packing of oligoacene.

Because the T_1 and T_2 dimers have similar coupling elements (0.137 and 0.120 eV) despite larger differences in distances (4.7 and 5.2 Å), we propose that a packing structure containing increased numbers of T_2 dimers might lead to a higher hole mobility. Figure 14a shows this type of structure. Each unit cell has two molecules, the center molecule overlaps half of the side molecules. This structure allows hole hopping between layers, which might dramatically improve mobility.

Because P dimer will be more stable than T_1 dimer at short distance (less than 4.9 Å), we propose that another packing structure only containing P dimers might also have an even higher hole mobility. Figure 14b shows this type of structure. The structure was minimized by the Dreiding force field. The optimum CM of P dimers in the crystal is 3.6 Å, leading to a coupling of 0.30 eV. Based on same method presented in section 3.2.1, the hole mobility of this structure will be 15.2 $cm^2/(V\ s)$, 2.8 times larger than the value of 5.37 $cm^2/(V\ s)$ for the normal crystal.

On the basis of eq 1, the second parameter, reorganization energy, depends exponentially on the hole mobility. Because smaller reorganization energies lead to larger hole mobilities, the design of new organic systems should consider adding groups that can delocalize the charges on the oligoacenes to help reduce the reorganization energy. Clearly adding additional aromatic groups to form hexacene and heptacene would lead to decreased reorganization energies as in eq 13 and hence larger mobilities.

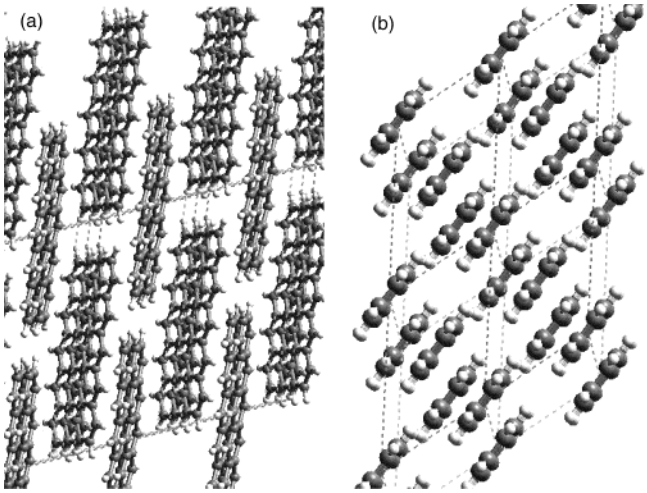

Figure 14. (a) Proposed cross layer crystal packing. (b) Proposed pure P type package crystal. Dreiding force field minimization gives the crystal structure with 1.343 g/cm^3 density and cell parameters a = 6.43 Å, b = 8.89 Å, c = 15.90 Å, α = 73.33°, β = 75.13°, and γ = 52.64°.

4. Conclusions

We present here a simple transport model to predict the drift mobility of oligoacenes from parameters deduced from QM calculations. In this model the drift mobility (μ) depends mainly on the monomer reorganization energy (λ) and the coupling matrix element (V) between dimers. Our result for pentacene (μ = 6.5 cm^2/(V s)) is close to those of the best experiments (μ = 3−7 cm^2/(V s)), validating our model. Note added in proof: A recent experiment (Jurchescu, O. D.; Baas, J.; Palstra, T. T. M. *Appl. Phys. Lett.* **2004**, *84*, 3061) reports a field effect hole mobility of 11.2 cm^2/s for very pure single crystals. This value is slightly higher than our value of 6.5 cm^2/s, perhaps indicating the role of coherent transport or possibly uncertainties due to the simplified methodology. However, it is in the range of disagreements of hole mobilities as measured by field effect and time of flight methods. Jurchescu also considered corrections of this directly measured value to estimate the inhomogeneous current flow, estimating that the limiting mobility for the basal plane is 35 cm^2/s.

We find that the drift mobility decreases around 9% (8.3% from 250 to 300 K, 9.2% from 300 to 350 K) with a 50 K increase in temperature due to reduced the electron coupling matrix elements. We find that an increased pressure of 1 GPa leads to only a 3.4% increase in the mobility. However, repacking the monomers to form a crystal dominated by P type dimers could lead to hole mobilities as high as 15.2 cm^2/(V s).

We suggest that this simple model might be useful for determining new solid-state structures that could lead to the higher hole mobility desired for high-performance molecular devices, and we suggest some alternative solid-state structures for such studies.

Acknowledgment. We thank Dr. Terry Smith (3M Corp.) for suggesting this as an interesting problem, and we thank 3M for a gift that helped support this work. This research was also supported partly by funds from the NSF S&T Center for Photonics (Larry Dalton, U. Washington). The computational facilities were provided by DURIP grants from ARO and ONR. The facilities of the Materials and Process Simulation Center are also supported by ONR, DOE (ASC, FETL), NSF, MURI-ARO, MURI-ONR, General Motors, ChevronTexaco, Seiko-Epson, Beckman Institute, and Asahi Kasei.

References and Notes

(1) Ye, J.; Chen, H. Z.; Shi, M. M.; Wang, M. *Prog. Nat. Sci.* **2003**, *13*, 81−87 and references therein.

(2) Dimitrakopoulos, C. D.; Malenfant, P. R. L. *Adv. Mater*. **2002**, *14*, 99−117 and references therein.

(3) Dimitrakopoulos, C. D.; Mascaro, D. J. *IBM J. Res. Dev.* **2001**, *45*, 11−27 and references therein.

(4) (a) Kelley, T. W.; Muyres, D. V.; Baude, P. F.; Smith, T. P.; Jones, T. D. *Mater. Res. Soc. Symp. Proc*. **2003**, *771*, L.6.5.1 (b) Klauk, H.; Halik, M.; Zschieschang, U.; Schmid, G.; Radlik, W.; Weber, W. *J. Appl. Phys*. **2002**, *92*, 5259.

(5) Cheng, Y. C.; Silbey, R. J.; da Silva Filho, D. A.; Calbert, J. P.; Cornil, J.; Bre'das J. L. *J. Chem. Phys.* **2003**, *118*, 3764−3774.

(6) Karl, N. *Synth. Met.* **2003**, *133*−*134*, 649−657.

(7) Silinsh E. A.; Capek V. *Organic Molecular crystals: interaction, localization and transport phenomena*; AIP Press: New York, 1994; pp 332−333.

(8) Senthilkumar, K.; Grozema, F. C.; Bickelhaupt, F. M.; Siebbelesb, L. D. A. *J. Chem. Phys*. **2003**, *119*, 9809.

(9) Wegewijs, B. R.; Siebbeles, L. D. A. *Phys. Rev. B* **2002**, *65*, 245112.

(10) Berlin, Y. A.; Hutchison, G. R.; Rempala P.; Ratner, M. A.; Michl, J. *J. Phys. Chem. A* **2003**, *107*, 3970−3980.

(11) (a) Marcus, R. *Annu. Rev. Phys. Chem*. **1964**, *15*, 155. (b) Bixon M.; Jortner *J. Adv. Chem. Phys*. **1999**, *106*, 35−208. (c) Bolton, J. R.; Mataga, N.; McLendon, G. In *Electron Transfer in Inorganic, Organic, and Biological Systems*; Bolton, J. R., Mataga, N., McLendon, G., Eds.; Advances in Chemistry Series No. 228; American Chemical Society: Washington, DC, 1991; (d) Bixon M.; Jortner J. *Adv. Chem. Phys*. **1999**, *106*, 35−208.

(12) (a) Burin, A. L.; Berlin, Y. A.; Ratner, M. A. *J. Phys. Chem. A* **2001**, 105. (b) D. Raineri, F. O.; Friedman, H. L. *Adv. Chem. Phys*. **1999**, *107*, 81. (c) Matyushov, D. V.; Voth, G. A. *J. Phys. Chem.* **1999**, *103*, 10981. (d) Tavernier, H. L.; Kalashnikov, M. M.; Fayer, M. D. *J. Chem. Phys.* **2000**, *113*, 10191. (e) Matyushov, D. V.; Voth, G. A. *J. Phys. Chem. A* **2000**, *104*, 6470. (f) Tavernier, H. L.; Fayer, M. D. *J. Chem. Phys*. **2001**, *114*, 4552.

(13) Jaguar 4.0 quantum mechanics program. Schodinger Inc., Portland, OR. See: Greeley, B. H.; Russo, T. V.; Mainz, D. T.; Friesner, R. A.; Langlois, J−M.; Goddard, W. A., III.; Donnelly, R. E.; Ringnalda, M. N. *J. Chem. Phys.* **1994**, *101*, 4028.

(14) (a) Marcus, R. *J. Chem. Phys.* **1956**, *24*, 966. (b) Hush, N. S. *J. Chem. Phys*. **1958**, *28*, 962. (c) Hush, N. S. *Trans. Faraday Soc*. **1961**, *57*, 577.

(15) Cerius2 molecular dynamics software. Accelrys Inc., San Diego CA.

(16) Mayo, S. L.; Olafson, B. D.; Goddard, W. A., III. *J. Phys. Chem*. **1990**, *94*, 8897.

(17) Mattheus, C. C.; de Wijs, G. A.; de Groot, R. A.; Palstra, T. T. M. *J. Am. Chem. Soc*. **2003**, *125*, 6323−6330.

(18) Karasawa N.; Goddard W. A., III. *J. Phys. Chem*. **1989**, *93*, 7320.

(19) Cambridge Structural Database. (a) (Naphthalene) Brock, C. P.; Dunitz, J. D. *Acta Crystallogr., Sect. B: Struct. Sci.* **1982**, *38*, 2218. (b) Anthracene: Brock, C. P.; Dunitz, J. D. *Acta Crystallogr., Sect. B: Struct. Sci.* **1990**, *46*, 795. (c) Tetracene and pentacene: Holmes, D.; Kumaraswamy, S.; Matzger, A. J.; Vollhardt, K. P. C. *Chem. Eur. J.* **1999**, *5*, 3399. http://www.ccdc.cam.ac.uk/products/csd/.

(20) (a) Coropceanu, V.; Malagoli, M.; da Silva Filho, D. A.; Gruhn, N. E.; Bill, T. G.; Bre'das J. L. *Phys. Rev. Lett*. **2002**, *89*, 275503. (b) Gruhn, N. E.; da Silva Filho, D. A.; Bill, T. G.; Malagoli, M.; Coropceanu, V.; Kahn, A.; Bre'das, J. L. *J. Am. Chem. Soc*. **2002**, *124*, 7918−7919.

(21) Ion Energetics Data in NIST Chemistry Webbook, NIST Standard Reference Database Number 69; Linstrom, P. J.; Mallard, W. G., Eds.; National Institute of Standards and Technology: Gaithersburg, MD, 2001 http://webbook.nist.gov.

(22) Chen, X. L.; Lovinger, A. J.; Bao, Z.; Sapjeta J. *Chem. Mater*. **2001**, *13*, 1341−1348.

(23) Butko, V. Y.; Chi, X.; Ramirez, A. P. *Solid State Commun.* **2003**, *128*, 431−434.

(24) de Boer, R. W. I.; Klapwijk, T. M.; Morpurgo, A. F. *Appl. Phys. Lett*. **2003**, *83*, 4345.

(25) Farina, L.; Brillante, A.; Della Valle, R. G.; Venuti, E.; Amboage, M.; Syassen, K. *Chem. Phys. Lett*. **2003**, *375*, 490−494

(26) (a) Podzorov, V.; Sysoev, S. E.; Loginova, E.; Pudalov, V. M.; Gershenson, M. E. *Appl. Phys. Lett*. **2003**, *83*, 3504. (b) Podzorov, V.; Pudalov, V. M.; Gershenson, E. *Appl. Phys. Lett*. **2003**, *82*, 1739.

(27) Demiralp, E.; Goddard, W. A., III. *Phys. Rev. B* **1997**, *56*, 907.